Disturbance observer-based control of a dual output LLC converter for solid state lighting applications

Please check the document version of this publication:

• A submitted manuscript is the version of the article upon submission and before peer-review. There can be important differences between the submitted version and the official published version of record. People interested in the research are advised to contact the author for the final version of the publication, or visit the DOI to the publisher's website.
• The final author version and the galley proof are versions of the publication after peer review.
• The final published version features the final layout of the paper including the volume, issue and page numbers.

Link to publication

Disturbance Observer-Based Control of a Dual Output LLC Converter for Solid State Lighting Applications

Maurice G. L. Roes, Jorge L. Duarte and Marcel A. M. Hendrix
Eindhoven University of Technology
Electromechanics and Power Electronics group
P.O. Box 513, 5600MB Eindhoven, The Netherlands

Abstract—Feedback sensor isolation is often an expensive necessity in power converters, for reasons of safety and electromagnetic compatibility. A disturbance observer-based control strategy for a dual-output resonant converter is proposed to overcome this problem. Current control of two LED loads is achieved through estimation rather than measurement. Robustness against temperature changes, which have significant impact on the behaviour of the LEDs, is achieved through estimation of offsets in the forward voltages of the LED-strings. The power converter and LEDs are modelled accurately to obtain a good estimation accuracy. The whole implementation is steered towards a low cost solution.

Index Terms—Disturbance observer, Light-emitting diodes, Linear-quadratic-Gaussian control, Modelling.

I. INTRODUCTION

Multi-coloured LED lighting applications are rapidly gaining in popularity. One solution to driving these multiple LED-strings can be found in the use of a multi-output power converter. Unfortunately though, most of these converter topologies have a large number of components and often suffer from cross-regulation effects. The resonant dual-output LLC converter [1] (figure 1), that is used in this project does not have these problems. It has a minimal component count and has two independently controllable outputs, able to supply power to asymmetric loads. The reader is directed to the aforementioned paper for more information on the principle of operation of the converter.

In a traditional current control strategy the output currents are measured and controlled via a feedback loop. This method has the disadvantage of requiring a form of isolation in the feedback path to provide an acceptable measure of safety. Furthermore, measuring currents adds to the cost of the total system (current transducers, Hall sensors), or decreases the converter's efficiency (shunt resistors) and is therefore often highly undesirable. Using state estimation [2]–[4] can resolve this problem by providing a means of estimating the output currents. The output currents are predicted by a 'state estimator', using a model of the system and information about the converter's switching frequency and duty cycle. Measurements of primary side variables are subsequently used to correct the estimation. This brings the possibility of using the natural isolation of the converter's transformer to obtain
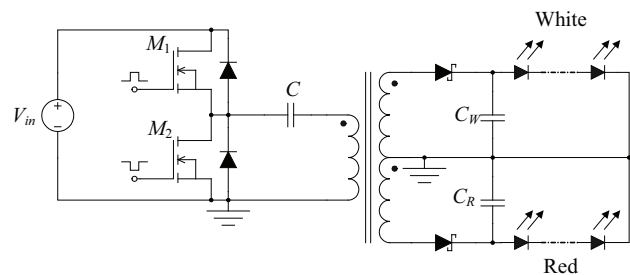

Figure 1. Dual output LLC converter with LED strings as load

the desired safety level, often referred to as primary sensing.

State estimators exist in a lot of different forms [2], however, the most used versions are Luenberger observers and Kalman filters, the latter being an optimal version of the former if additive zero mean, white noise Gaussian disturbances are present. The application of state estimators to resonant power converters is a whole new domain, with only a handful of publications on the subject to date (for example [5], [6]). Currently, these only consider situations that are not very likely to occur in practical situations (purely Ohmic loads, DSPs using very high sample rates, etcetera). This paper tries to fill these voids by using a more realistic application, while solving the innate problems.

The following sections discuss the design of a disturbance observer-based control strategy, aimed at the exclusive use of low cost hardware, which inherently implies that the AD conversion and processing use low sample rates. The goal is to regulate the average LED currents to within 5% of their reference values. The setup of the paper is as follows; first the modelling of the system is addressed. Next the implementation of the Linear-Quadratic-Gaussian control (LQG) algorithm for the estimation and control is discussed. Finally some experimental results are presented.

II. MODELLING

The key to accurate estimation of the average LED currents is to have a good model of the process that is being observed (i.e., the converter and the LEDs). In the following subsections the different parts of the model will be discussed.
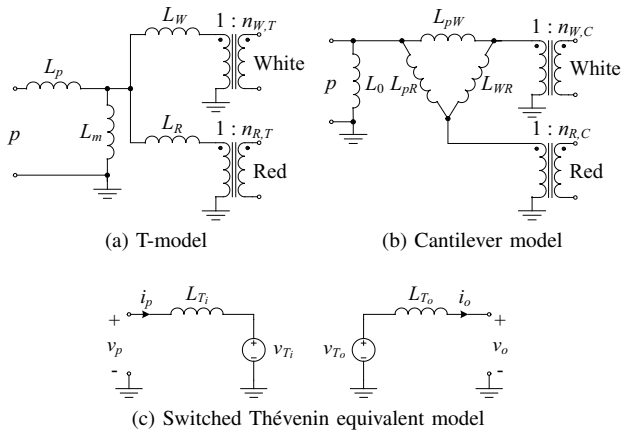
(a) T-model   (b) Cantilever model

(c) Switched Thévenin equivalent model

Figure 2.   Transformer models

Figure 3.   Switch functions for the high side ($q_H(t)$) and low side ($q_L(t)$) MOSFETs

(a) White LED-string   (b) Red LED-string

Figure 4.   Static and transient voltage-current characteristics of the LED-strings

A. Converter

A closer examination of figure 1 reveals six switching elements, of which only two (MOSFETs M_1 and M_2) are controlled externally. This causes the operation of the converter to be fairly complicated. Hence the derivation of its model is not straightforward.

1) Transformer: The transformer plays a critical role in the operation of the converter, since its magnetising and leakage inductances define the resonant frequencies. The most used models for a three winding transformer are the extended T-model, shown in figure 2a, as used in [1] and the cantilever-, or Δ-model [7] of figure 2b. A resistance R_0 is added across the primary winding to account for core losses in the transformer. The conduction losses are assumed negligible.

Because the secondary windings of the transformer are designed to have a high coupling factor and they are connected to rectifier diodes (see figure 1), the two outputs of the converter cannot carry a current at the same time. Therefore both models can be transformed to the Thévenin equivalent circuit of figure 2c. In this representation the values of L_{T_i}, v_{T_i}, L_{T_o} and v_{T_o} are switched, depending on which of the output rectifier diodes in figure 1 is conducting.

The Thévenin parameters cannot be measured directly, so either the T or Δ-model will have to be used to extract them. See table I for the conversion from cantilever model parameters to those of the Thévenin model. A similar table can be derived for the T-model.

Since the currents through L_{T_i} and L_{T_o} are continuous at the switching instants they can be used as state variables. This model is used, because it has the advantage of a reduction in the number of state variables needed from three to two.

2) Half bridge: The half bridge operation is modelled by including a dead time t_d between the driving signals (see figure 3). This also requires including the parasitic drain-source capacitances C_{DS} of M_1 and M_2. Their charge-discharge cycle defines the midpoint voltage when neither the MOSFETs nor their body diodes conduct. The on-state resistance R_{DS} of the MOSFETs is included to model losses due to conduction.
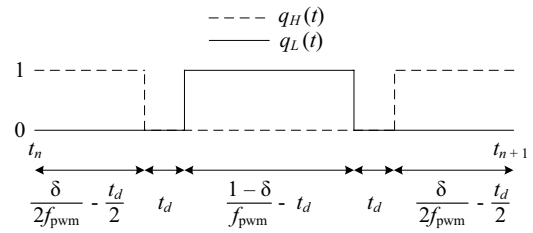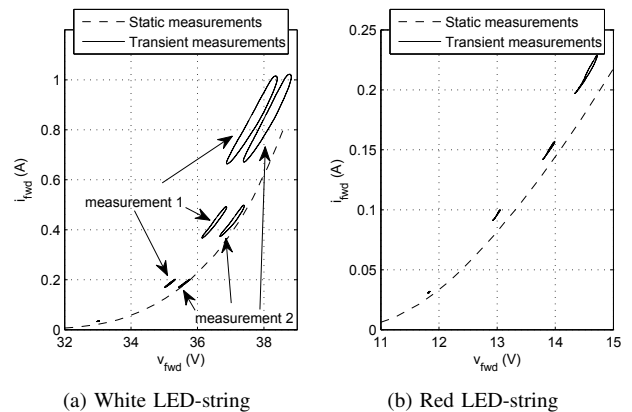
B. LEDs

Two LED strings, composed of 12 white and 6 red series connected Luxeon Rebel LEDs respectively, are used for this project. Two different voltage patterns have been applied for their modelling. A static measurement using an adjustable constant forward voltage yields the dashed lines in figure 4. Their exponential characteristic resembles the behaviour of a normal diode, and is therefore modelled with the Shockley diode equation [8]

$$i_{\text{fwd}}(v_{\text{fwd}}) = I_s \left(e^{\frac{v_{\text{fwd}}}{NV_T}} - 1 \right) \tag{1}$$

in which I_s is the reverse bias saturation current, N the emission coefficient, V_T the thermal voltage and v_{fwd} the forward voltage. A series resistance R_s is added to account for the resistive behaviour of contacts and internal connections. A transient measurement has been done to examine the behaviour of the LEDs when a ripple is present on the forward voltage. The results are shown as solid lines in the graphs. The forward voltage was supplied by the dual output converter and therefore contained a ripple at the switching frequency, as shown for instance in figure 5. The ellipsoidal shapes of the transient measurement graphs in figure 4 are caused by a phase lag between voltage and current. The current proved to be lagging the voltage and is hence modelled using a series inductance L_s. This strikes as odd, since one would expect capacitive behaviour due to the junction capacitance of the diode as explained in [8].

Somewhat disturbing is the voltage shift between the static and transient measurements (they should lie on top

Table I
CONVERSION TO THÉVENIN PARAMETERS FROM THE CANTILEVER MODEL

m_o *	1	2	3
L_{T_i,m_o}	$\dfrac{1}{\frac{1}{L_0}+\frac{1}{L_{pW}}+\frac{1}{L_{pR}+L_{WR}}}$	$\dfrac{1}{\frac{1}{L_0}+\frac{1}{L_{pR}}+\frac{1}{L_{pW}+L_{WR}}}$	L_0
v_{T_i,m_o}	$\dfrac{L_0}{L_0+\frac{L_{pW}(L_{pR}+L_{WR})}{L_{pW}+L_{pR}+L_{WR}}}\dfrac{v_o}{n_{W,C}}$	$-\dfrac{L_0}{L_0+\frac{L_{pR}(L_{pW}+L_{WR})}{L_{pW}+L_{pR}+L_{WR}}}\dfrac{v_o}{n_{R,C}}$	0
L_{T_o,m_o}	$n_{W,C}^2\dfrac{L_{pW}(L_{pR}+L_{WR})}{L_{pW}+L_{pR}+L_{WR}}$	$n_{R,C}^2\dfrac{L_{pR}(L_{pW}+L_{WR})}{L_{pW}+L_{pR}+L_{WR}}$	undefined
v_{T_o,m_o}	$n_{W,C}\,v_p$	$-n_{R,C}\,v_p$	undefined

* – m_o DEFINES WHICH OUTPUT DIODE CONDUCTS; '1' FOR THE WHITE OUTPUT, '2' FOR THE RED OUTPUT AND '3' FOR NEITHER.

of each other) and between the different areas of the transient measurements. An explanation is found when examining a second set of transient measurements, included in figure 4a, where the current amplitudes and average values are matched to those of the first measurements. This shows that the voltage-current relationship has a time varying component, most likely due to changes in the ambient temperature. The shift for increasing forward current can be attributed to a change in temperature as well, although the LEDs are cooled with a fan and a heat sink to keep their temperature as constant as possible.

The effects of changing forward voltages will be compensated using a disturbance observer. More on this subject can be found in section III-A.

The single LED model allows the whole string to be modelled as one LED. Its parameters can be found by fitting the model to transient measurement data, from which the following parameters are obtained;

$$I_{s,W} = 1.86 \cdot 10^{-20}\,\text{A}, \quad I_{s,R} = 5.85 \cdot 10^{-17}\,\text{A},$$
$$N_W = 30.5, \quad N_R = 13.5,$$
$$R_{s,W} = 3.90\,\Omega, \quad R_{s,R} = 10.8\,\Omega,$$
$$L_{s,W} = 634\,\text{nH}, \quad L_{s,R} = 891\,\text{nH}.$$

The subscripts W and R indicate the white and red strings respectively. Using the fitted parameters, the simulated currents (i_{mod}) show a very good resemblance to the measured currents (i_m) as can be seen in figure 5.

C. Complete large signal description

The models of the transformer, the half bridge and the LEDs can be combined into one large signal model, depicted in figure 6. The output diodes have been modelled with a constant forward voltage drop of $V_{D_o,W}$ and $V_{D_o,R}$ during their conduction. The complete model can then be represented by the switched differential equations

$$\begin{pmatrix} \dot{\mathbf{x}}_l(t) \\ \dot{\mathbf{x}}_{nl}(t) \end{pmatrix} =$$
$$\left(\begin{pmatrix} \mathbf{A}_{\text{in},m_i} \\ \mathbf{A}_{\text{out},m_o} \end{pmatrix} \begin{pmatrix} \mathbf{x}_l(t) \\ \mathbf{x}_{nl}(t) \end{pmatrix} + \begin{pmatrix} \mathbf{B}_{\text{in},m_i} \\ \mathbf{B}_{\text{out},m_o} \end{pmatrix} \mathbf{u}(t) \\ \mathbf{f}\left(\mathbf{x}_l(t),\mathbf{x}_{nl}(t)\right) \right),$$
$$m_i, m_o \in \{1,2,3\} \quad (2)$$
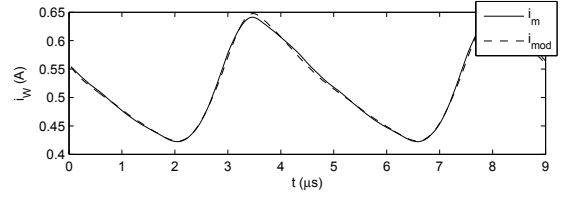
(a) White LED current i_W
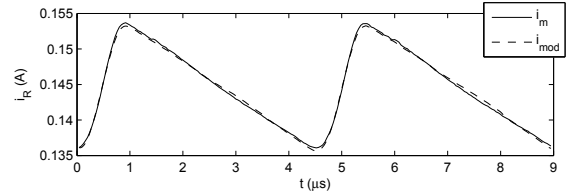
(b) Red LED current i_R

Figure 5. Measured LED current (i_m) and simulated LED current (i_{mod}) waveforms after parameter fitting

dividing the state vector into a linear and a nonlinear part, i.e., $\mathbf{x}(t) = (\mathbf{x}_l(t),\ \mathbf{x}_{nl}(t))^{\text{T}}$, with

$$\mathbf{x}_l(t) = \begin{pmatrix} v_x(t) \\ v_C(t) \\ i_p(t) \\ i_o(t) \\ v_{C_W}(t) \\ v_{C_R}(t) \end{pmatrix}, \quad \mathbf{x}_{nl}(t) = \begin{pmatrix} i_W(t) \\ i_R(t) \\ \langle i_W \rangle(t) \\ \langle i_R \rangle(t) \end{pmatrix}.$$

The individual state variables are indicated in figure 6. The input vector $u(t)$ is defined as

$$\mathbf{u}(t) = \begin{pmatrix} V_{in}, & V_{D_o,W}, & V_{D_o,R} \end{pmatrix}^{\text{T}}.$$

The switch functions of the half bridge are depicted in figure 3. These can be written as

$$q_H(t) = \begin{cases} 1, & t_n - \frac{\delta}{2f_{\text{pwm},n}} + \frac{1}{2}t_d < t \le t_n + \frac{\delta}{2f_{\text{pwm},n}} - \frac{1}{2}t_d \\ 0, & \text{otherwise} \end{cases}$$

$$q_L(t) = \begin{cases} 1, & t_n + \frac{\delta}{2f_{\text{pwm},n}} + \frac{1}{2}t_d < t \le t_n + \frac{2-\delta}{2f_{\text{pwm},n}} - \frac{1}{2}t_d \\ 0 & \text{otherwise} \end{cases}$$

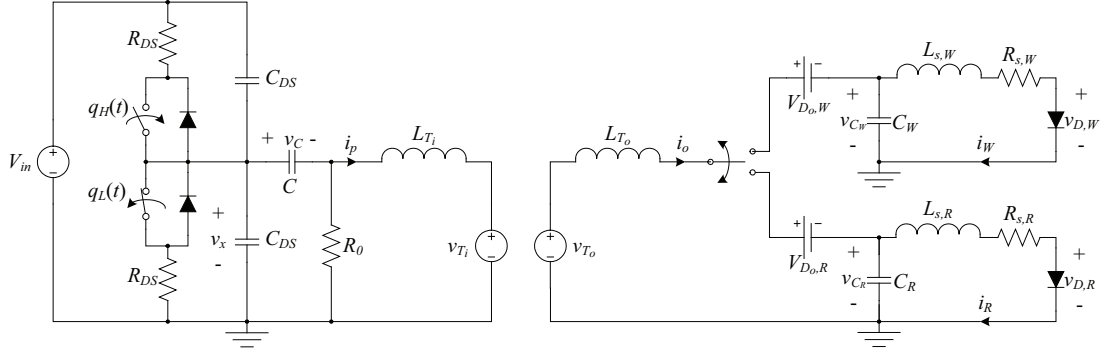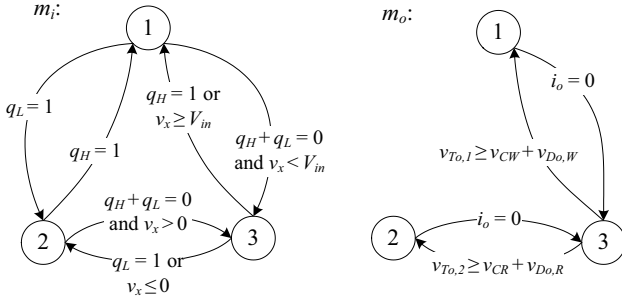$$n \in \mathbb{Z}, \quad t_{n+1} - t_n = \frac{1}{f_{\text{pwm},n}}.$$

Figure 6.   Complete converter model

Figure 7.   State transition diagrams for $m_i(t)$ and $m_o(t)$

The variable m_i in (2) is defined as being '1' when the high side MOSFET (or its body diode) conducts, '2' when the low side MOSFET is conducting and '3' when neither carries current. Variable m_o has a similar definition. It is '1' when the 'white' output diode conducts and '2' when the 'red' output diode conducts and '3' in 'idle' mode. This is depicted in the state transition diagrams of figure 7.

Table I shows that the Thévenin equivalent primary and secondary voltages can be written as

$$v_{T_i,m_o}(t) = N_{T_i,m_o} v_o(t)$$
$$v_{T_o,m_o}(t) = N_{T_o,m_o} v_p(t) \quad , \qquad m_o \in \{1,2\} \ .$$

This renders the derivation of the matrices $\mathbf{A}_{\mathrm{in},m_i}$, $\mathbf{B}_{\mathrm{in},m_i}$, $\mathbf{A}_{\mathrm{out},m_o}$ and $\mathbf{B}_{\mathrm{out},m_o}$ in (2) pretty straightforward. The results are shown in table II.

Lastly, the nonlinear part of state space model (2) can now be defined as

$$\mathbf{f}\left(\mathbf{x}_l(t), \ \mathbf{x}_{nl}(t)\right) = \begin{pmatrix} \frac{di_W(t)}{dt} \\ \frac{di_R(t)}{dt} \\ f_{\mathrm{pwm}} \, i_W(t) \\ f_{\mathrm{pwm}} \, i_R(t) \end{pmatrix},$$

in which the derivatives of the LED currents are given by

$$\frac{di_\gamma(t)}{dt} = \frac{1}{L_{s,\gamma}} \Big(v_{C_\gamma}(t) - i_\gamma(t) R_{s,\gamma} - \cdots$$
$$\cdots \frac{N_\gamma}{V_T} \ln\left(\frac{i_\gamma(t)}{I_{s,\gamma}} + 1\right) - v_{\mathrm{os},\gamma}(t) \Big),$$
$$\gamma \in \{W, R\},$$

The variables $v_{\mathrm{os},W}$ and $v_{\mathrm{os},R}$ give the LED strings an offset in their forward voltages. This addition to the model

will be used in section III-A to counter the uncertainty in these variables, as observed in section II-B. On top of that, these offsets can be used to cancel the spreading on forward voltages that occurs in the production process.

The state variables $\langle i_W \rangle$(t) and $\langle i_R \rangle$(t) are reset to zero every $T_{\mathrm{pwm},n}$ seconds at $t = t_n$ so that they represent a cyclic average of the LED currents, i.e.,

$$\langle i_{\gamma,n} \rangle = f_{\mathrm{pwm}} \int_{t_{n-1}}^{t_n} i_\gamma(t)dt, \qquad \gamma \in \{W, R\} \ .$$

D. Discrete time modelling

Discrete time models for switched linear systems are usually created by means of state averaging [9] or zero-order-hold modelling [10].

These methods are both ill-suited for this converter. Therefore the small signal model is derived by numerical differentiation from (2). Doing so will result in a discrete time model of the form

$$\tilde{\mathbf{x}}_{n+1} = \mathbf{F}_0 \tilde{\mathbf{x}}_n + \mathbf{G}_0 \tilde{\mathbf{u}}_n + \mathbf{H}_0 \mathbf{v}_{\mathrm{os},n} , \qquad (3)$$

the tilde denoting a deviation from steady state, i.e.,

$$\tilde{\mathbf{x}}_n = \mathbf{x}_n - \mathbf{x}^{\mathrm{ss}}, \qquad \tilde{\mathbf{u}}_n = \mathbf{u}_n - \mathbf{u}^{\mathrm{ss}}.$$

and the vector $\mathbf{u}_n$ containing the input variables of the system;

$$\mathbf{u}_n = \begin{pmatrix} \delta_n, & f_{\mathrm{pwm},n}, & V_{\mathrm{in},n} \end{pmatrix}^{\mathrm{T}}. \qquad (4)$$

The vector of offset voltages $\mathbf{v}_{\mathrm{os}}$ for the LED strings (defined in section II-C) is used in (3) as a disturbance input for the discrete time system.

The discrete time representation (3) is a Zero-Order-Hold model, of which the sampling frequency equals the switching frequency. The instants t_n are defined in figure 3 and should satisfy

$$T_{\mathrm{pwm},n} = \frac{1}{f_{\mathrm{pwm},n}} = t_{n+1} - t_n \quad \forall n \in \mathbb{Z}, \qquad (5)$$

and thus the sampling rate of the model changes with the switching frequency.

The Jacobian matrices $\mathbf{F}_0$, $\mathbf{G}_0$ and $\mathbf{H}_0$ in (3) are found through numerical differentiation of $\mathbf{x}(t)$, which is in turn obtained using an ODE solver on the continuous time model equations (2). The numerical differentiation can be summarised as follows; $\mathbf{x}_n$ is set to the steady state value

TABLE II
STATE SPACE MATRICES

m_i	$\mathbf{A}_{\mathrm{in},m_i}$	$\mathbf{B}_{\mathrm{in},m_i}$
1	$\begin{pmatrix} -\frac{R_{DS}+R_0}{2C_{DS}R_{DS}R_0} & \frac{1}{2C_{DS}R_0} & -\frac{1}{2C_{DS}} & \mathbf{0} \\ \frac{1}{CR_0} & -\frac{1}{CR_0} & \frac{1}{C} & \end{pmatrix}$	$\begin{pmatrix} \frac{1}{2C_{DS}R_{DS}} & \mathbf{0} \\ 0 & \end{pmatrix}$
2	$\begin{pmatrix} -\frac{R_{DS}+R_0}{2C_{DS}R_{DS}R_0} & \frac{1}{2C_{DS}R_0} & -\frac{1}{2C_{DS}} & \mathbf{0} \\ \frac{1}{CR_0} & -\frac{1}{CR_0} & \frac{1}{C} & \end{pmatrix}$	$\mathbf{0}$
3	$\begin{pmatrix} -\frac{1}{2C_{DS}R_0} & \frac{1}{2C_{DS}R_0} & -\frac{1}{2C_{DS}} & \mathbf{0} \\ \frac{1}{CR_0} & -\frac{1}{CR_0} & \frac{1}{C} & \end{pmatrix}$	$\mathbf{0}$

(a) INPUT MATRICES A_{in,m_i} AND B_{in,m_i}

m_o	$\mathbf{A}_{\mathrm{out},m_o}$	$\mathbf{B}_{\mathrm{out},m_o}$
1	$\begin{pmatrix} \frac{1}{L_{T_i,1}} & -\frac{1}{L_{T_i,1}} & 0 & 0 & -\frac{N_{T_i,1}}{L_{T_i,1}} & 0 & 0 & 0 \\ \frac{N_{T_o,1}}{L_{T_o,1}} & -\frac{N_{T_o,1}}{L_{T_o,1}} & 0 & 0 & -\frac{1}{L_{T_o,1}} & 0 & 0 & 0 \\ 0 & 0 & 0 & \frac{1}{C_W} & 0 & 0 & -\frac{1}{C_W} & 0 \\ 0 & 0 & 0 & 0 & 0 & 0 & 0 & -\frac{1}{C_R} \end{pmatrix}$	$\begin{pmatrix} 0 & -\frac{N_{T_i,1}}{L_{T_i,1}} & 0 \\ 0 & -\frac{1}{L_{T_o,1}} & 0 \\ & \mathbf{0} & \end{pmatrix}$
2	$\begin{pmatrix} \frac{1}{L_{T_i,2}} & -\frac{1}{L_{T_i,2}} & 0 & 0 & 0 & -\frac{N_{T_i,2}}{L_{T_i,2}} & 0 & 0 \\ \frac{N_{T_o,2}}{L_{T_o,2}} & -\frac{N_{T_o,2}}{L_{T_o,2}} & 0 & 0 & 0 & -\frac{1}{L_{T_o,2}} & 0 & 0 \\ 0 & 0 & 0 & 0 & 0 & 0 & -\frac{1}{C_W} & 0 \\ 0 & 0 & 0 & \frac{1}{C_R} & 0 & 0 & 0 & -\frac{1}{C_R} \end{pmatrix}$	$\begin{pmatrix} 0 & 0 & -\frac{N_{T_i,2}}{L_{T_i,2}} \\ 0 & 0 & -\frac{1}{L_{T_o,2}} \\ & \mathbf{0} & \end{pmatrix}$
3	$\begin{pmatrix} \frac{1}{L_{T_i,3}} & -\frac{1}{L_{T_i,3}} & 0 & 0 & 0 & 0 & 0 & 0 \\ 0 & 0 & 0 & 0 & 0 & 0 & 0 & 0 \\ 0 & 0 & 0 & 0 & 0 & 0 & -\frac{1}{C_W} & 0 \\ 0 & 0 & 0 & 0 & 0 & 0 & 0 & -\frac{1}{C_R} \end{pmatrix}$	$\mathbf{0}$

(b) OUTPUT MATRICES A_{out,m_o} AND B_{out,m_o}

$\mathbf{x}^{\mathrm{ss}}$ for which the small signal model should be derived, and a sufficiently small perturbation Δx^i is added to its i-th state variable. Using the ODE solver with initial value $\mathbf{x}_n$ to calculate $\mathbf{x}_{n+1}|_{\Delta x^i}$, the column vector of derivatives in (6) results:

$$\frac{\partial \mathbf{x}_{n+1}}{\partial x_n^i} = \frac{\mathbf{x}_{n+1}\Big|_{\Delta x^i} - \mathbf{x}_{n+1}\Big|_{-\Delta x^i}}{2\Delta x^i}. \tag{6}$$

A positive and a negative perturbation are applied to improve the accuracy, especially in combination with errors in $\mathbf{x}^{\mathrm{ss}}$. These are effectively cancelled in this way. The Jacobian matrix can now be defined as

$$\mathbf{F}_0 = \begin{pmatrix} \frac{\partial \mathbf{x}_{n+1}}{\partial x_n^1} & \frac{\partial \mathbf{x}_{n+1}}{\partial x_n^2} & \cdots & \frac{\partial \mathbf{x}_{n+1}}{\partial x_n^{10}} \end{pmatrix}.$$

$\mathbf{G}_0$ and $\mathbf{H}_0$ are obtained in an analogous fashion.

The use of a cheap DSP poses a limit on the rate at which calculations and AD conversions can be performed, and therefore restricts this sampling period $T_{s,k}$ (defined analogously to (5)) to lie well below the switching period. Synchronous sampling will be used to reduce switching noise in the AD conversion process, meaning that a frequency ratio n_f is introduced, such that

$$f_s(t) = \frac{f_{\mathrm{pwm}}(t)}{n_f}, \quad n_f \in \mathbb{Z}_+,$$

which leads to the definition of a new model at sample rate $f_{s,k} = \frac{1}{T_{s,k}}$:

$$\tilde{\mathbf{x}}_{k+1} = \mathbf{F}\tilde{\mathbf{x}}_k + \mathbf{G}\tilde{\mathbf{u}}_k + \mathbf{H}\mathbf{v}_{\mathrm{os},k}. \tag{7}$$

It can be shown that (7) can be found from (3) by means of extrapolation over n_f switching periods while keeping $\tilde{\mathbf{u}}_n$ and $\mathbf{v}_{\mathrm{os},n}$ constant. This yields

$$\mathbf{F} = (\mathbf{F}_0)^{n_f}, \quad \mathbf{G} = \sum_{l=0}^{n_f-1}(\mathbf{F}_0)^l\,\mathbf{G}_0, \quad \mathbf{H} = \sum_{l=0}^{n_f-1}(\mathbf{F}_0)^l\,\mathbf{H}_0, \tag{8}$$

which is essentially the same as downsampling the model by a factor n_f.

E. Model reduction

The numerical differentiation described in (6) results in a discrete time system with the same number of state variables as the continuous time system. Not all of those variables are necessary for an accurate representation. Therefore balanced model truncation [3], [4] is applied. This yields a reduced order representation that closely resembles the original model.

The above results in a new discrete time model

$$\tilde{\mathbf{x}}_{r,k+1} = \mathbf{F}_r\tilde{\mathbf{x}}_{r,k} + \mathbf{G}_r\tilde{\mathbf{u}}_k + \mathbf{H}_r\mathbf{v}_{\mathrm{os},k}. \tag{9}$$

A Hankel singular value decomposition [4] of the model (7) reveals that it can be accurately described using a fourth order model. This has been verified using simulations.

III. ESTIMATION & CONTROL

Linear-Quadratic-Gaussian control with an extension to a disturbance observer is used for the control of the

dual output converter. An LQG controller is essentially a combination of a Kalman filter and a Linear-Quadratic Regulator (LQR).

A. Kalman filter

A Kalman filter [3], [4] is used to estimate the average output currents. Kalman filters are intended to be used in systems with additive, zero mean white noise; it is suboptimal with regard to rejection of persistent disturbances. Normally these are cancelled to some extent, because of the propagation of the measurements through the state vector $\tilde{\mathbf{x}}_{r,k}$ by the model (9). Unfortunately, the relatively high value of n_f that is used ($n_f = 15$) in (8) causes this propagation to be very small; the influence of the $\mathbf{F}\tilde{\mathbf{x}}_k$ term in (7) is much smaller than that of $\mathbf{G}\tilde{\mathbf{u}}_k$. In this project we are dealing with disturbances (the offset voltages $\mathbf{v}_{\mathrm{os}}$) that can be treated as being more or less constant. Hence the Kalman filter needs to be extended to a disturbance observer [3] by defining an augmented model

$$\tilde{\mathbf{z}}_k = \begin{pmatrix} \tilde{\mathbf{x}}_{r,k} \\ \mathbf{v}_{\mathrm{os},k} \end{pmatrix}$$

$$\tilde{\mathbf{z}}_{k+1} = \begin{pmatrix} \mathbf{F}_r & \mathbf{H}_r \\ \mathbf{0} & \mathbf{I} \end{pmatrix} \tilde{\mathbf{z}}_k + \begin{pmatrix} \mathbf{G}_r \\ \mathbf{0} \end{pmatrix} \tilde{\mathbf{u}}_k + \begin{pmatrix} \mathbf{0} \\ \mathbf{I} \end{pmatrix} \mathbf{w}_k$$

$$\tilde{\mathbf{y}}_{m,k} = \mathbf{C}_m \tilde{\mathbf{z}}_k + \mathbf{D}_m \tilde{\mathbf{u}}_k + \mathbf{v}_k$$

$$\tilde{\mathbf{y}}_{p,k} = \mathbf{C}_p \tilde{\mathbf{z}}_k + \mathbf{D}_p \tilde{\mathbf{u}}_k \,,$$

where $\tilde{\mathbf{y}}_{m,k}$ is a vector of measurements and $\tilde{\mathbf{y}}_{p,k}$ the vector of average output currents $\left(\langle \tilde{i_W} \rangle_k, \ \langle \tilde{i_R} \rangle_k \right)^{\mathrm{T}}$. The vectors $\mathbf{w}_k$ and $\mathbf{v}_k$ are the process and measurement noise, with respective covariance matrices $\mathbf{Q}_K$ and $\mathbf{R}_K$. The process noise on the state vector $\tilde{\mathbf{x}}_{r,k}$ is defined to be zero because of the limited sample rate of the model, also limiting the noise bandwidth. The process noise covariance matrix $\mathbf{Q}_K$ therefore only has components for the offset voltages $v_{\mathrm{os},W,k}$ and $v_{\mathrm{os},R,k}$, which are modelled as being uncorrelated (although strictly speaking that is not true). Therefore $\mathbf{Q}_K$ is a diagonal matrix.

The resulting Kalman estimator is given by the discrete time system

$$\hat{\tilde{\mathbf{z}}}_{k+1|k} = \mathbf{A}_K \hat{\tilde{\mathbf{z}}}_{k|k-1} + \mathbf{B}_{K,u} \tilde{\mathbf{u}}_k + \mathbf{B}_{K,y} \tilde{\mathbf{y}}_{m,k}$$

$$\hat{\tilde{\mathbf{y}}}_{p,k|k} = \mathbf{C}_K \hat{\tilde{\mathbf{z}}}_{k|k-1} + \mathbf{D}_{K,u} \tilde{\mathbf{u}}_k + \mathbf{D}_{K,y} \tilde{\mathbf{y}}_{m,k}$$

$$\mathbf{A}_K = \begin{pmatrix} \mathbf{F}_r & \mathbf{H}_r \\ \mathbf{0} & \mathbf{I} \end{pmatrix} (\mathbf{I} - \mathbf{M}_k \mathbf{C}_m)$$

$$\mathbf{B}_{K,u} = \begin{pmatrix} \mathbf{G}_r \\ \mathbf{0} \end{pmatrix} - \begin{pmatrix} \mathbf{F}_r & \mathbf{H}_r \\ \mathbf{0} & \mathbf{I} \end{pmatrix} \mathbf{M}_k \mathbf{D}_m$$

$$\mathbf{B}_{K,y} = \begin{pmatrix} \mathbf{F}_r & \mathbf{H}_r \\ \mathbf{0} & \mathbf{I} \end{pmatrix} \mathbf{M}_k \,, \qquad \mathbf{C}_K = \mathbf{C}_p \left(\mathbf{I} - \mathbf{M}_k \mathbf{C}_m \right)$$

$$\mathbf{D}_{K,u} = \mathbf{D}_p - \mathbf{C}_p \mathbf{M}_k \mathbf{D}_m \,, \quad \mathbf{D}_{K,y} = \mathbf{C}_p \mathbf{M}_k \,,$$

where the 'hat' notation indicates an estimate of the concerning state variables.

The notation implies that the Kalman gain $\mathbf{M}_k$ is updated at each instant t_k. This, however, brings no extra performance if the initial estimation error covariance is unknown and only increases the processor load. Therefore a steady state Kalman gain $\mathbf{M}_k = \mathbf{M}$ is used.

The estimation of the output currents has been made robust against input voltage disturbances by measuring $V_{\mathrm{in},k}$ and including it in the definition of $\tilde{\mathbf{u}}_k$ in (4), hence it is accounted for in the estimation through $\mathbf{B}_{K,u}$ and $\mathbf{D}_{K,u}$.

B. Measurements

Practical low cost implementations of low bandwidth measurements are limited to average values, peak values and phase relations of primary variables. The only primary measurements that can be performed that hold enough low-frequency information about the secondary currents are the average input current $\langle i_{\mathrm{in}} \rangle$ through M_1, and the phase relation ϕ between v_x and i_p. Unfortunately, from simulations it became clear that ϕ suffers heavily from nonlinearity.

Since the state variables $\mathbf{v}_{\mathrm{os}}$ are uncontrollable and defined as being uncorrelated, estimating them requires at least two measurements with orthogonal components. Consequently other measurements will have to be used. A solution is found in measuring the output voltages v_{C_W} and v_{C_R} via large impedances (1 MΩ) to introduce some isolation between primary and secondary side. The parasitic low pass behaviour of such large resistances is of no concern since filtering is required anyhow to prevent aliasing.

The measurement noise is assumed to originate only from quantisation, since synchronous sampling is applied. It can be approximated with uniformly distributed noise, yielding the covariance matrix [11]

$$\mathbf{R}_K = \mathrm{diag} \left(\frac{1}{12} \left(\frac{v_{C_W}^{\max}}{2^b} \right)^2, \quad \frac{1}{12} \left(\frac{v_{C_R}^{\max}}{2^b} \right)^2 \right),$$

with b the number of available bits for the AD conversion.

C. Linear-quadratic regulator

LQR control [3] is typically aimed at MIMO systems, such as the converter under study and is therefore well suited for the control problem at hand.

The LQR used for tracking the current reference uses a slightly modified version of the discrete time model (9). Because V_{in} in (4) is a measurement and cannot be changed by the LQR, another model definition is necessary, requiring the introduction of the input vector

$$\tilde{\mathbf{u}}'_k = \begin{pmatrix} \tilde{\delta}_k \\ \tilde{f}_{\mathrm{pwm},k} \end{pmatrix}, \quad \text{and hence} \quad \mathbf{G}_r = \begin{pmatrix} \mathbf{G}_1, & \mathbf{G}_2 \end{pmatrix}.$$

Moreover, an integrating part is added to the model to allow for reference tracking and to be able to cancel other than zero mean white noise disturbances [3]. This results in a model

$$\begin{pmatrix} \tilde{\mathbf{x}}_{r,k+1} \\ \mathbf{e}_{k+1} \end{pmatrix} = \begin{pmatrix} \mathbf{F}_r & \mathbf{0} \\ -\mathbf{C}_p & \mathbf{I} \end{pmatrix} \begin{pmatrix} \tilde{\mathbf{x}}_{r,k} \\ \mathbf{e}_k \end{pmatrix} + \\ \begin{pmatrix} \mathbf{G}_1 \\ -\mathbf{D}_p \end{pmatrix} \tilde{\mathbf{u}}'_k + \begin{pmatrix} \mathbf{0} \\ \mathbf{I} \end{pmatrix} \tilde{\mathbf{r}}_k \,, \quad (10)$$

where the current reference is defined as

$$\tilde{\mathbf{r}}_k = \mathbf{r}_k - \mathbf{y}_p^{\mathrm{ss}} \qquad \mathbf{r}_k = \begin{pmatrix} \langle i_W \rangle^{\mathrm{ref}} \\ \langle i_R \rangle^{\mathrm{ref}} \end{pmatrix}.$$

The LQR design yields a feedback gain vector $\mathbf{K}_k$ of which the time varying character again gives no extra performance. Hence a steady state gain vector $\mathbf{K}$ is used. The LQR is designed for the model (10), neglecting the reference term, by setting the cost function to

$$J = \sum_{k=0}^{\infty} \left(\begin{pmatrix} \tilde{\mathbf{x}}_{r,k} & \mathbf{e}_k \end{pmatrix} \begin{pmatrix} \mathbf{0} & \mathbf{0} \\ \mathbf{0} & \mathbf{Q}_R \end{pmatrix} \begin{pmatrix} \tilde{\mathbf{x}}_{r,k} \\ \mathbf{e}_k \end{pmatrix} + \tilde{\mathbf{u}}_k'^{\mathrm{T}} \mathbf{R}_R\, \tilde{\mathbf{u}}_k' \right),$$

with diagonal state and input weighting matrices $\mathbf{Q}_R$ and $\mathbf{R}_R$. This definition only puts weight on the integral error term $\mathbf{e}_k$. The elements of $\mathbf{Q}_R$ and $\mathbf{R}_R$ are found by setting their order of magnitude according to those of the currents and input variables (squared), and subsequently tweaking them for optimal performance.

The feedback control law that results is

$$\tilde{\mathbf{u}}_k' = -\mathbf{K} \begin{pmatrix} \tilde{\mathbf{x}}_{r,k} \\ \mathbf{e}_k \end{pmatrix} = - \begin{pmatrix} \mathbf{K}_x & \mathbf{K}_e \end{pmatrix} \begin{pmatrix} \tilde{\mathbf{x}}_{r,k} \\ \mathbf{e}_k \end{pmatrix}.$$

To keep the system causal, this is implemented as

$$\tilde{\mathbf{u}}_k' = - \begin{pmatrix} \mathbf{K}_x & \mathbf{K}_e \end{pmatrix} \begin{pmatrix} \hat{\tilde{\mathbf{x}}}_{r,k|k-1} \\ \sum_{l=0}^{k-1} \left(\tilde{\mathbf{r}}_l - \hat{\tilde{\mathbf{y}}}_{p,l|l} \right) \end{pmatrix}. \qquad (11)$$

This implementation has the advantage that the steady state converges to the corrector term $\hat{\tilde{\mathbf{y}}}_{p,k|k}$, rather than the predictor term $\hat{\tilde{\mathbf{y}}}_{p,k|k-1}$ of the Kalman filter. Modelling errors are thereby cancelled to some extent. The advantage of this approach especially shines when using a large value for the model downsampling ratio n_f.

## IV. EXPERIMENTAL RESULTS

A. Implementation

A dSpace 1104 system is used to run the LQG algorithm and perform the AD conversion of v_{C_W} and v_{C_R}. Two differential amplifiers, based on a cheap TL072 dual opamp IC, are used to amplify the output voltages to the right level. A dedicated FPWM (frequency and pulse-width modulation) module is implemented on a Xilinx Virtex4 FPGA. Its limited time resolution shows in the graphs in this section as quantisation in the current amplitudes.

The prototype converter used in this project uses a switching frequency between 200 kHz and 300 kHz and is designed for a total output power of 40 W.
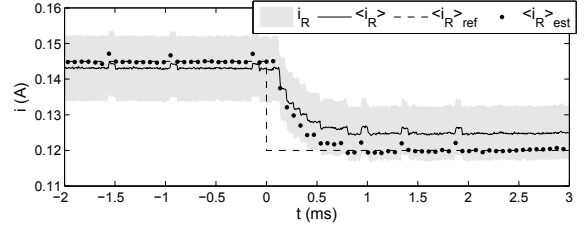
The estimation of the disturbances $\hat{\mathbf{v}}_{\mathrm{os},k|k-1}$ is kept slow, because only slow changes in the offsets are to be expected during normal operation. Good results were achieved using

$$\mathbf{Q}_K = \begin{pmatrix} 10^{-6} & 0 \\ 0 & 5 \cdot 10^{-7} \end{pmatrix}, \qquad \mathbf{Q}_R = \begin{pmatrix} 1 & 0 \\ 0 & 40 \end{pmatrix},$$

$$\mathbf{R}_K = \begin{pmatrix} 3 \cdot 10^{-5} & 0 \\ 0 & 5 \cdot 10^{-6} \end{pmatrix}, \qquad \mathbf{R}_R = \begin{pmatrix} 800 & 0 \\ 0 & 8 \cdot 10^{-9} \end{pmatrix}.$$
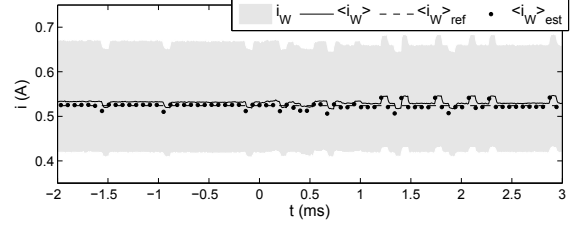
(a) White LED current

(b) Red LED current

Figure 8.   Response to a step in the red LED current reference from $\langle i_R \rangle^{\mathrm{ref}} = 145\,\mathrm{mA}$ to $\langle i_R \rangle^{\mathrm{ref}} = 120\,\mathrm{mA}$ at $t = 0\,\mathrm{s}$

B. Step response

The tracking capability of the Kalman filter and the LQR is examined by applying a step in the current reference. The results for a step in $\langle i_R \rangle^{\mathrm{ref}}$, while keeping $\langle i_W \rangle^{\mathrm{ref}}$ constant are shown in figures 8a (i_W) and 8b (i_R).

The graphs show that the average output currents are estimated very well in the chosen model's operating point

$$\mathbf{y}_p^{\mathrm{ss}} = \begin{pmatrix} \langle i_W \rangle^{\mathrm{ss}} \\ \langle i_R \rangle^{\mathrm{ss}} \end{pmatrix} = \begin{pmatrix} 524 \\ 145 \end{pmatrix} \mathrm{mA}\,.$$

After settling to the new reference, the error in $\langle i_R \rangle$ is small, while the error in the $\langle i_W \rangle$ is completely negligible.

C. Temperature change

By letting the LEDs heat up and then cooling them down, the influence of a change in temperature is investigated. The results are shown in figure 9. As can be expected, the offset voltage estimates increase exponentially with the cooling of the LEDs [8] (see figure 9c). The control and estimation of $\langle i_W \rangle$ is virtually uninfluenced by the temperature change (figure 9a). The current through the red LEDs is affected to a larger extent (figure 9b), although the estimation error is negligible again after a long time (not shown).

D. LED short circuit

Since most LED failure mechanisms lead to a short circuit behaviour [12], it is interesting to investigate how the closed loop system responds to such a sudden change. Seeing that the dynamic resistance of an LED is very low, an LED short circuit can be modelled to a reasonable extent by a forward voltage offset $v_{\mathrm{os}} \approx -V_{\mathrm{fwd}}$. Consequently, the designed LQG algorithm should be able to compensate for the short circuit of an LED. The graphs of figure 10 prove that this is indeed the case. Figure 10c shows that $\hat{v}_{\mathrm{os},W}$ falls by approximately 3V after the short circuit occurs, which is the forward voltage of one LED.
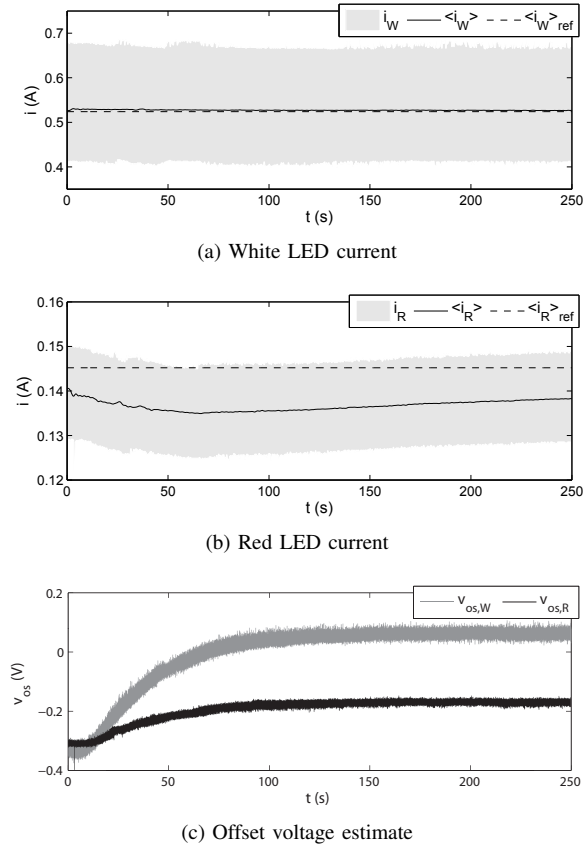
(a) White LED current

(b) Red LED current

(c) Offset voltage estimate

Figure 9.   System response to a change in temperature

(a) White LED current

(b) Red LED current

(c) Offset voltage estimate

Figure 10.   System response to a short circuit of one of the white LEDs at $t = 0$ s

An error remains in i_R once a steady state is reached (see figure 10b), although the estimation of $\langle i_W \rangle$ is again excellent (figure 10a). This error originates from the fact that the system's model is no longer accurate enough, due to the change in the dynamic resistance of the white LED-string.
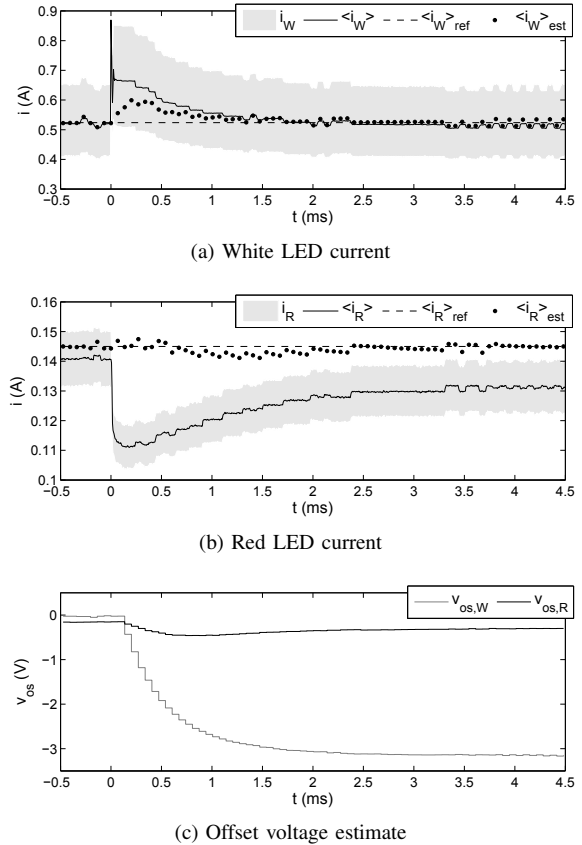
V.   CONCLUSIONS

A control scheme based on an LQG algorithm has been proposed to control a resonant dual-output LLC converter driving two individual LED loads. The extension of the Kalman filter to a disturbance observer allows the estimation of a voltage offset in the forward voltages of the LED-strings, thereby enabling the controller to nullify the effects of temperature changes without actually measuring the temperature. The uncertainty in the proposed LED model is minimised in this way.

Due to the use of model order reduction and low sample rates, the solution is extremely well suited for low cost implementations. Results from tests with a prototype converter showed that the algorithm works perfectly, especially in the model's operating point. Outside the operating point, moderate errors in the estimation are present due to linearisation of the model. The goal of regulation within 5% accuracy is attainable within a limited operating range.

REFERENCES

[1] R. Elferich and T. Dürbaum, "A new load resonant dual-output converter," in *Proc. IEEE Power Electronics Specialists Conf.*, June 2002, pp. 1319–1324.

[2] A. Radke and Z. Gao, "A survey of state and disturbance observers for practitioners," in *Proc. American Control Conf.*, June 2006, pp. 5183–5188.

[3] J. B. Burl, *Linear optimal control: $\mathcal{H}_2$ and $\mathcal{H}_\infty$ methods*. Menlo Park, CA: Addison-Wesley, 1999.

[4] M. Green and D. J. N. Limebeer, *Linear robust control*. Englewood Cliffs, NJ: Prentice-Hall, Inc., 1995.

[5] A. J. Gilbert, C. M. Bingham, B. S. Bhangu, M. P. Foster, and D. A. Stone, "EKF-based output-voltage regulation of 3rd-order LCC resonant converters subject to load variations," in *Proc. European Conf. on Power Electronics and Applications*, September 2005, pp. 1–8.

[6] A. Hultgren, W. Kulesza, and M. Lenells, "Switched Kalman filter in a high frequency series loaded resonant converter," in *Proc. IEEE Int. Conf. Control Applications*, September 2000, pp. 507–512.

[7] K. D. T. Ngo, "Improved method to extract the short-circuit parameters of the BECM," *IEEE Power Electronics Letters*, vol. 1, no. 1, pp. 17–18, March 2003.

[8] D. A. Neamen, *Semiconductor physics and devices*, 3rd ed. Hoboken, NJ: McGraw-Hill, 2002.

[9] N. Mohan, T. M. Undeland, and W. P. Robbins, *Power electronics: converters, applications, and design*, 3rd ed. New York, NY: John Wiley and Sons Inc., 2003.

[10] J. L. Duarte, "Small-signal modelling and analysis of switching converters using MATLAB," *Int. journal of electronics*, vol. 85, no. 2, pp. 231–269, August 1998.

[11] B. Widrow, I. Kollár, and M.-C. Liu, "Statistical Theory of Quantization," *IEEE Transactions on instrumentation and measurement*, vol. 45, no. 2, pp. 353–361, April 1996.

[12] N. Hwang, "Failure analysis matrix of light emitting diodes for general lighting applications," in *Proc. Int. Symposium on the Physical and Failure Analysis of Integrated Circuits*, July 2008, pp. 1–4.